EXPERIMENTAL AND NUMERICAL INVESTIGATION OF RAYLEIGH-BENARD CONVECTION IN RECTANGULAR CAVITY WITH MOTOR OIL

by

Predrag M. ŽIVKOVIĆ[a], Mladen A. TOMIĆ[b*], Sadoon AYED[c], Cristian BARZ[d], and Drago SEVER[e]

[a] Faculty of Mechanical Engineering, University of Niš, Niš, Serbia
[b] Faculty of Technical Sciences, Novi Sad, Serbia
[c] University of Technology, Baghdad, Iraq
[d] Northern University Center Baia Mare, University of Cluj-Napoca, Baia Mare, Romania
[e] Faculty of Civil Engineering, Transportation and Architecture, Maribor, Slovenia

Original scientific paper
https://doi.org/10.2298/TSCI230607216Z

Naturally flows have been the scope of the scientific research for centuries, Rayleigh-Benard convection being one of the leading. Many researchers have considered the flow patterns, boundary conditions, various cavities, nanofluids, theoretically, numerically, and experimentally. The flow was investigated in atmosphere and in nanofluids, in air, water, molten metals, non-Newtonian fluids. Almost all research focuses on 2-D or 3-D analysis of flow in laterally unlimited enclosures, as parallel plates or coaxial cylinders. In technical practice, only limited enclosures exist. This paper presents numerical and real experimental results for the test chamber with ratio 4×2×1 in x-, y-, and z-direction, respectfully. The measurements were taken at fifteen different positions on the faces of the tank. Probes used are PT100 elements. As the chamber is limited in all directions, the results have shown strong influence of the lateral walls. The results are compared with the those obtained by IR camera. Various fluids were tested, and results for motor oil will be presented.

Key words: *Rayleigh-Benard convection, temperature profile, PT100 probe, motor oil, numerical simulation*

Introduction

One of the simplest cases of fluid-flow is a laminar flow. Laminar flow exists until the flow parameters (*i.e.* the Reynolds number) do not reach a critical value. In supercritical parameters the laminar flow becomes unstable. Even the small disturbances can cause large changes so that it can not be maintained as originated, so becomes turbulent. Turbulent flow is extremely unstable, and its mathematical modelling most often extremely complex. The criterion determining the fluid-flow change (or retains the existing state) is called the stability criterion. This criterion is very important in fluid mechanics. In fluids that are exposed to disturbance, even the smallest instabilities can cause the transition from laminar to turbulent state. The theory of linear stability in fluid mechanics gives the criteria for obtaining the critical Reynolds number at which the fluid-flow becomes instable.

* Corresponding author, e-mail: mladen.tomic@uns.ac.rs

Natural convection in enclosed spaces has been studied extensively. It has a very wide range, from the smallest scales (in pipelines, channels, and tanks) to the largest ones (atmosphere, the molten planet core). The governing processes depend on the thermodynamic state and geometry of the respective surfaces, which defines the type of flow that can occur. A special group of these flows happens in the fluid between parallel plates with different temperatures. Most often the temperature of the lower plate is higher than of the upper plate – well known Rayleigh-Benard convection. Experimentally, the flow was explained by Henri Claude Benard. Lord Rayleigh pioneered the theoretical background, using the temperature gradient. As such, the domain top and bottom boundary conditions imply the disappearance of the vertical velocity component, which is not predicted by the Benard experiment. Authors in [1-3] proposed the model based on surface tension, which agrees with the experiment, *i.e.* the physical reality. Presented examples assumes that the plates that confines the fluid are unlimited. In engineering this is not the case, so the side walls influence on the flow, without idealization and in the real 3-D domain are important.

Although the mathematical model is complex, with some generalization, the effect of the instability on the turbulent flow structure can be predicted. Basic example of the Rayleigh-Benard convection is for a thin layer of fluid heated from below, limited by two parallel plates. The buoyancy forces caused by the temperature differences in the fluid layers are forming the flow. Depending on the flow parameters, different structures (named cells in 2-D and rolls in 3-D) are formed in the fields of temperature, velocity and vorticity. The Rayleigh-Benard problem in its simplest form and the basic treatment, is the special case of the infinite layer, when the fluid is limited by two infinite horizontal plates. The surfaces are not very (relatively) distant, as forming of structures caused by viscous effects can be expected in the vertical direction. The heating of a lower plate has a negative temperature gradient (the density is lower at the bottom than on the top). Flow with the denser fluid at the top is potentially unstable. Natural fluid tendency to move influenced by the buoyancy forces will be disrupted due to the viscosity and heat dissipation, if the temperature gradient is below a critical value. Thermal instability occurs when the negative temperature is over the critical value.

Cell formation is usual for the systems which are far from the equilibrium state. The imbalance can be caused by different physical mechanisms – the fluid temperature, electrical potential difference or chemical reactions. Each driving force has a dissipation mechanism (*i.e.* viscosity) which opposes the system unbalancing. The cell formation is the result of the driving force and the dissipation mechanism balance. Cells can have different shapes (circular, square, hexagonal, spiral, stripes...).

From the application viewpoint, the thermal driving forces are of paramount importance. Examples are thermal convection in the atmosphere [4], in the oceans [5], including thermohaline convection [6], thermal convection in buildings [7, 8], in chemical industry, metallurgy [9], and the like. In geophysics and astrophysics, we can mention the convection in the Earth mantle [10], Earth outer core of [11], the stars, including the Sun [12]. Convection is also associated with the formation and disappearance of the geomagnetic field [13].

Mathematical modelling of the cell formation is carried out by means of the reduced equations. These equations are derived based on symmetry, which brings a complex mathematical model down to a form that is characteristic for the most physical systems. Examples of basic symmetry: discrete translational 1-D symmetry (for systems that form cells in the form of stripes) and discrete translational 2-D symmetry (for systems that form square cells). As examples of the reduced equations we can take the Ginzburg-Landau

equations, which describe systems with translational invariant, with the pattern in the form of stripes [14-16].

These equations are called reduced since they reduce the degree of the system independence by removing fast variables and by modelling slow ones. As fast variables conditionally follow the change of slow variables, the slow variables are all that is needed to model the entire system. An example is the formation of cells in the form of stripes. Fast variables describe the cell in the form of stripes for a wave number, k, while the slow variables describe the amplitude and phase modulation, which causes the formation of such cells.

Applying the reduced equations gives significant results in predicting the linear stability of uniform periodic fluid states with varied control parameter. The reduced equation theory has also shown good results in the description of coherent structures, such as dislocations and domain walls. Rayleigh-Benard convection played a key role in the hydrodynamics stability theory development [17, 18], but is also paradigmatic in model forming and the study of time and space chaos [19, 20].

That is why the researchers have been studying the Rayleigh-Benard system for almost a century – it is important for many applications, ranging from astrophysics (for example, when the value of a star model depends, to a large extent, on external regions of stellar atmospheres), geophysics (current theories of continental drift depend on the possible convection movements in the earth's mantle, caused by heat, generated internally by the radioactive decay), and the science of the atmosphere (theory and forecasting of current weather conditions, as well as long-term effects such as ice age, depend on the value of the convection energy transport theory in the Earth atmosphere). This system application to various technical systems, such as solar energy systems, materials processing, energy storage and nuclear systems, are numerous.

The *standard* mathematical model of the Rayleigh-Benard system consists of a series of non-linear combined PDE that ca not be solved by the classical mathematical apparatus. This model can give valuable data in the non-linear systems research. Rayleigh-Benard system is one of the most carefully studied case of self-organizing non-linear systems, which are vital for the research in the field of Synergetics. Model forming very similar to spatial-temporal models can be seen in the creation of crystals, solidifying propagation fronts, electrodynamic instability and liquid crystals, chemical reaction-diffusion process, auto-catalytic reactions, deformation of thin plates and shells, morphogenesis of plants and animals, *etc.*

Experimental studies have considered different shapes of chambers – parallelepiped, cylindrical, spherical, trapezoidal, *U*-shape [21-38], various fluids (Newtonian and non-Newtonian), with nanoparticles [26, 27, 38-41], *etc.* Along the experimental, many numerical studies have been performed. All kinds of methods were used, such as direct numerical simulation [16, 24, 25, 42, 43], simulations of large eddies or averaged Navier-Stokes equations [44, 45], with boundary layer treatment [46-56]. The Rayleigh-Benard convection, as reported in [57], can be considered as *the forefather of the canonical examples that were used for the study of model forming and behavior in extended systems in space*. It provides opportunity to study the spontaneous spatial ordering and simultaneously raises the question of the flow special shape and size feasibility, or the desirable shape, and proportion selection.

This paper is concerned with the lateral walls influence [58], while most studies are concerned with infinite or semi-infinite domains where the chamber test measurements with air were presented. As the velocity is in the range 1-10 mm/s, the temperatures were measured, while the velocities were simulated. The chamber was made in order to minimize

the disturbances of the flow, and the upper and lower plates to be of practically uniform temperature.

Mathematical modelling

Thermal-flow processes are described by the system of conservation equations of matter, momentum, and energy. In addition, the system of equations, primarily for fluids with no constant density, also consists of relations, as for the fluid state. In some simple cases, such as the Stokes flow, the equation can be simplified to the level of linear equations. However, in all real situations those equations are difficult or impossible to solve, so we resort to simplification or modelling.

Transport equations

The partial differential equation describing the mass, momentum and energy transfer phenomena expresses the principle of conservation for a given transport quantity. The equations of conservation are [58]:

– Mass conservation equation:

$$\frac{\partial \rho}{\partial \tau} + \frac{\partial (\rho u_i)}{\partial x_i} = 0 \tag{1}$$

– Momentum conservation equations – Navier-Stokes equations:

$$\frac{\partial (\rho u_i)}{\partial \tau} + \frac{\partial (\rho u_i u_j)}{\partial x_j} = \frac{\partial (\tau_{ij})}{\partial x_j} - \frac{\partial p}{\partial x_i} + f_i \tag{2}$$

– Energy conservation equation:

$$\frac{\partial (\rho h)}{\partial \tau} + \frac{\partial (\rho u_i h)}{\partial x_i} = \frac{\partial (j_{ih})}{\partial x_i} + \mu \Phi + S_h \tag{3}$$

where ρ is the density, u_i – the velocity components, p – the pressure, f_i – the momentum equations source terms (volume, Coriolis, buoyancy forces, *etc.*), h – the enthalpy, S_h – the production/destruction of energy, and j_{ih} – the diffusive energy transport fluxes. In Newtonian fluids the tensor, τ_{ij}, has the following form:

$$\tau_{ij} = \mu \left(\frac{\partial u_i}{\partial x_j} + \frac{\partial u_j}{\partial x_i} \right) - \mu \frac{2}{3} \frac{\partial u_k}{\partial x_k} \delta_{ij} \tag{4}$$

where μ is the dynamic viscosity of the fluid, δ_{ij} – the Kronecker delta operator ($\delta_{ij} = 1$ for $i = j$ and $\delta_{ij} = 0$ for $i \neq j$).

In eq. (3) diffusive flux of energy transport, j_{ih}, includes energy transport by conduction and viscous dissipation. This can be expressed:

$$j_{ih} = \Gamma_{\mathrm{T}} \frac{\partial T}{\partial x_i} \tag{5}$$

where

$$\Phi = \frac{1}{2} \left(\frac{\partial u_i}{\partial x_j} + \frac{\partial u_j}{\partial x_i} \right)^2 - \frac{2}{3} \frac{\partial u_k}{\partial x_k} \frac{\partial u_i}{\partial x_i} \tag{6}$$

and $\Gamma_{\mathrm{T}} = \lambda$ is the thermal conductivity, the diffusion coefficient for enthalpy ($h = c_p T$).

For incompressible fluids, the change of density can be presented in the linear form as a function of temperature, with β as a compressibility factor of dimension K^{-1}:

$$\rho = \rho_0[1 - \beta(T - T_0)] \tag{7}$$

If $p = p_0 + p'$, $\rho = \rho_0 + \rho'$ and the body forces f_i are replaced by ρg_i, eq. (2) becomes:

$$(\rho_0 + \rho')\left[\frac{\partial u_i}{\partial \tau} + \frac{\partial(\rho u_i u_j)}{\partial x_j}\right] = \mu \frac{\partial}{\partial x_j}\left(\frac{\partial u_i}{\partial x_j} + \frac{\partial u_j}{\partial x_i}\right) - \frac{\partial p_0}{\partial x_i} + \rho_0 g_i + \rho' g_i \tag{8}$$

and noting that in the hydrostatics $\partial p_0/\partial x_i = \rho_0 g_i$, and, finally, dividing with ρ_0:

$$\left(1 + \frac{\rho'}{\rho_0}\right)\left[\frac{\partial u_i}{\partial \tau} + \frac{\partial(\rho u_i u_j)}{\partial x_j}\right] = \nu \frac{\partial}{\partial x_j}\left(\frac{\partial u_i}{\partial x_j} + \frac{\partial u_j}{\partial x_i}\right) - \frac{1}{\rho_0}\frac{\partial p'}{\partial x_i} + \frac{\rho'}{\rho_0} g_i \tag{9}$$

For small values of density fluctuation, ρ' can be neglected. If $p = p_0 + p'$, then $dp = dp'$, and considering the density dependence on temperature, we obtain:

$$\frac{\partial u_i}{\partial \tau} + \frac{\partial(\rho u_i u_j)}{\partial x_j} = \nu \frac{\partial}{\partial x_j}\left(\frac{\partial u_i}{\partial x_j} + \frac{\partial u_j}{\partial x_i}\right) - \frac{1}{\rho_0}\frac{\partial p_0}{\partial x_i} + g_i \beta \Delta T \tag{10}$$

By introducing the dimensionless quantities for velocity U, time τ, pressure and temperature, $\overline{p}$ and $\overline{T}$, and length $\overline{x}$ we obtain:

$$\frac{1}{\mathrm{Pr}}\left[\frac{\partial U_i}{\partial \tau} + \frac{\partial(\rho U_i U_j)}{\partial \overline{x}_j}\right] = \frac{\partial^2 U_i}{\partial \overline{x}_J^2} - \frac{\partial \overline{p}}{\partial \overline{x}_i} + \mathrm{Ra}\overline{T} \tag{11}$$

where $\mathrm{Pr} = \nu/a$ represents the Prandtl number. The Rayleigh number Ra, (analogous to the Reynolds number) is the buoyancy and the viscous forces ratio:

$$\mathrm{Ra} = \frac{g\beta\Delta T L^3}{\nu a} \tag{12}$$

Experimental set-up

Experiment presented in this paper is performed with motor oil. The turbulent regime transition occurs for $\mathrm{Ra} \sim 10^6$ in oil. In the investigation presented, Rayleigh number range was $2.58 \times 10^7 < \mathrm{Ra} < 5.59 \times 10^7$. The turbulent regime can be assumed for all experiments. The tank used is shown in fig. 1, sized 500 mm × 250 mm × 125 mm, in *x*-, *y*-, and *z*-axis, respectively. Distance between the hated and the cooled plate is the *z*-direction dimension [58].

Experimental data

In order to achieve as precise results as possible, experiment lasted some five days, at different ambient temperatures. Long term and the representative stable hourly measurements are presented in fig. 2. The curve TS01 represents the temperature of the heated plate. As presented, daily temperature change is about 2 °C to 4 °C. Maximum hourly change is 0.2 °C, which is approximately the probe precision. The daily variation of the ambient temperature is between 4 °C and 7 °C (max 0.2 °C per hour, curve TS16). Control measurements were performed with IR camera [58].

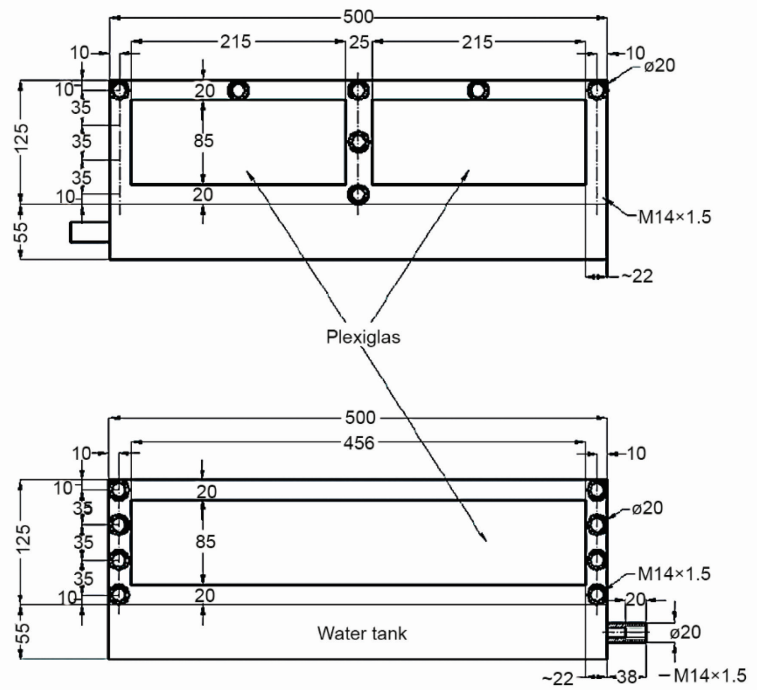

Figure 1. Measuring points on the tank lateral sides disposition (vertical projection)

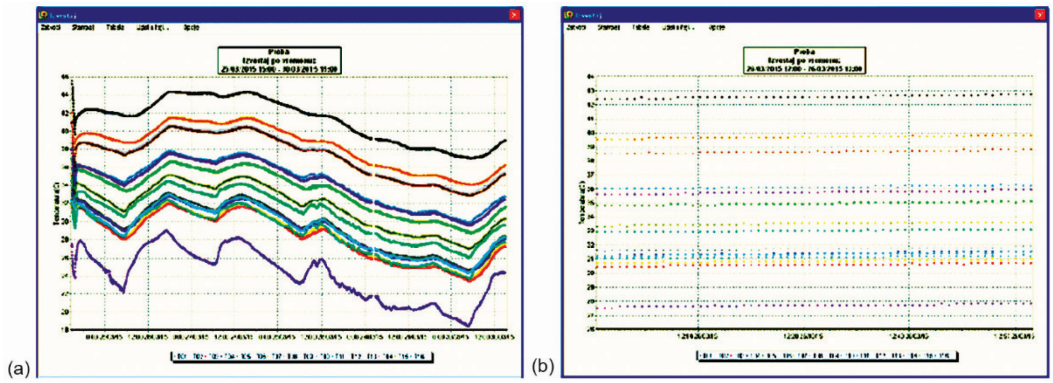

Figure 2. Long term (a) and selected stable hourly measurements (b)
(*for color image see journal web site*)

Parallel measurements with IR camera were performed. The measurement lasted for 4 minutes. The probe temperature change due to insulation removing (up to 0.4 °C) can be neglected, due to the somewhat larger probe inertia. One can assume that the temperature change is due to increased convection, caused by increased air velocity in the room, from door opening, people entering or exiting the test room during measurements, insulation removing and reapplying, *etc*.

Numerical procedure

Transport equations of dependent variables can be presented in the generalized form:

$$\frac{\partial(\rho\Phi)}{\partial t}+\frac{\partial(\rho u_j\Phi)}{\partial x_j}=\frac{\partial}{\partial x_i}\left(\Gamma_\Phi\frac{\partial\Phi}{\partial x_i}\right)+S_\Phi \tag{13}$$

where Γ_Φ is the diffusion coefficient and S_Φ – the source term. Expression forms for Γ_Φ and S_Φ depend on the variable Φ. For most models, incompressibility assumption is taken, so the equations of continuity, momentum, energy, k and ε, can be represented by mentioned general transport equation.

Numerical experiment was performed using the software package PHOENICS 2011.

Numerical model

Turbulence model equations

$$U_j\frac{\partial k}{\partial x_j}-\frac{\partial}{\partial x_j}\left[\left(\nu+\frac{\nu_T}{\sigma_k}\right)\frac{\partial k}{\partial x_j}\right]=P_k-\varepsilon \tag{14}$$

$$U_j\frac{\partial \varepsilon}{\partial x_j}-\frac{\partial}{\partial x_j}\left[\left(\nu+\frac{\nu_T}{\sigma_\varepsilon}\right)\frac{\partial \varepsilon}{\partial x_j}\right]=\frac{\varepsilon}{k}(C_{\varepsilon 1}P_k-C_{\varepsilon 2}\varepsilon) \tag{15}$$

where $\nu_{\text{eff}}=\nu+\nu_T$, $\nu_T=C_\mu k^2/\varepsilon$, so:

$$P_k=\nu_T\left(\frac{\partial U_i}{\partial x_j}+\frac{\partial U_j}{\partial x_i}\right)\frac{\partial U_i}{\partial x_j} \tag{16}$$

Discretization scheme selection

For choosing the low Reynolds number k-ε, *RNG* k-ε, and k-ω model were considered that are embedded in the software package used, PHOENICS 2011. With proper adjustment, all the models gave good results. However, since the RNG k-ε model does not require such a fine mesh as low Reynolds number k-ε, and therefore is faster, it is adopted for use. A summary of the model is given in tab. 1.

The chamber, whose 3-D model is shown in fig. 3 is sized 125 mm × 250 mm × 500 mm, according to the size of the experimental chamber. Since the chamber is insulated laterally, in the numerical set it is assumed that the side walls are adiabatically insulated, while the upper and the lower sides are assumed to be at a constant temperature in accordance to the measured values, while the heat transfer is modelled with logarithmic wall functions. For the mesh selection, computer resources and the dimensionless parameter y^+ were considered. Generally, the grid is refined towards the walls so that it complies with the requirements of wall function $y^+ < 30$. The Cartesian grid is selected with 100 × 50 × 25 cells in the x-, y-, and z-directions, respectively. Time step is determined in accordance with the referential velocity and length, so that for the upward flow (the case of RBC), there is minimum of 5 time-steps.

Table 1. Summary of the renormalized group - RNG *k-ε* model

Transport equation	Φ	Γ_Φ	S_Φ
Continuity	1	0	0
Momentum	u_i	ν	$-\frac{\partial p}{\partial x_j}-\frac{\partial(\rho\overline{u_i u_j})}{\partial x_i}$
Energy	h	λ	0
Kinetic energy of turbulence	k	ν_t/σ_k	$\rho(G-\varepsilon)$
Disipation of kinetic energy of turbulence	ε	ν_t/σ_ε	$\rho\frac{\varepsilon}{k}(C_{1\varepsilon}G-C^*_{2\varepsilon})$
$G=\nu_t(\partial_k u_i+\partial_i u_k)\partial_k u_i$			$\nu_t=C_\mu k^2/\varepsilon$
$(\sigma_k, \sigma_\varepsilon, C_{1\varepsilon}, C_{2\varepsilon}, C_u, \eta_0)=(0.7194, 0.7194, 1.42, 1.68, 0.0845, 0.012)$			

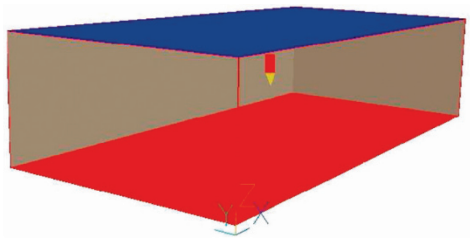

Figure 3. Isometry of the 3-D model

Results of numerical simulations for RBC

At the very beginning the vortices begin to form along the walls of the chamber. By further heating the fluid, after ~ 15 seconds, plumes begin to form, fig. 4(f) with typical velocities in the order of ~ 0.01 m/s. After the contact with the upper surface, the mixing of the fluid in the vessel and the formation of quasi-repetitive convective structures of RBC occur. For the case of motor oil, the complete formation of convective structures ends in the first 150 seconds. Figure 4 shows the velocity, temperature and pressure fields in the case of the chamber with oil after 1800 seconds. One can easily spot the formation of quasi-symmetrical convective structures, with a tendency of oscillatory repetitions.

Comparison of the measured and simulated results for RBC

The temperature probes were arranged in three or four positions in three different vertical sections. Such arrangement allows experimenting with various fluids and varying temperature regimes. Experiment has shown that relatively small changes of the ambient air temperature allowed the cooler plate to be directly exposed to the ambient. The measuring system appropriately responded to external disturbances [58]. The temperature probe design somewhat increased measurement inertia, which, on the other hand, allowed control IR camera measurements and using various fluids.

Validation of the numerical model is done by comparing the numerical and real experiment results, fig. 5. Deviations of results that occur in numerical simulation are the result of input errors, model errors, discretization errors, numerical errors, approximations of the actual geometry, *etc*., and are mostly under 0.5 °C, which corresponds to the numerical error in the range of 1-8%.

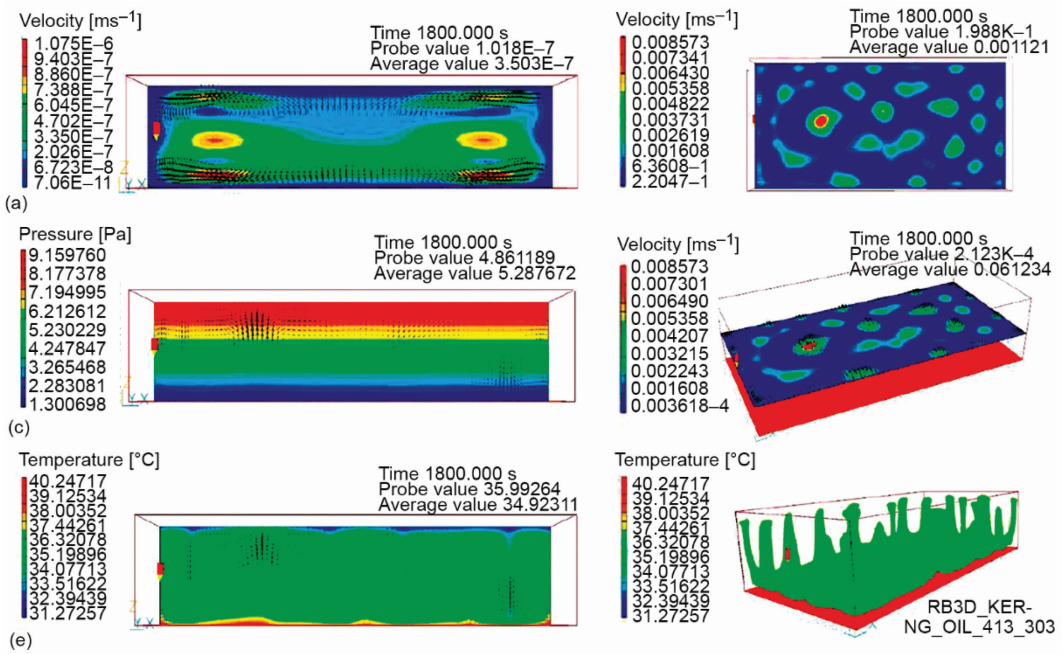

Figure 4. Velocity field in *x-z* plane (a), *x-y* plane (b), axonometric view (d); as well as the pressure field (c), temperature field (e), RBC structures (f); for the chamber with oil for plate temperatures TS01 = 41.3 °C and TS16 = 30.3 °C (used as boundary conditions)

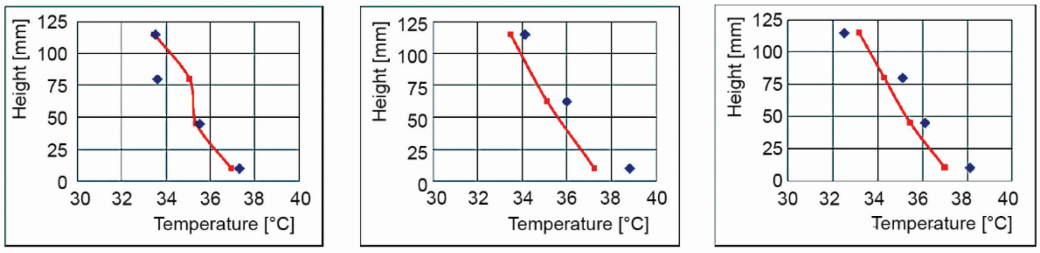

Figure 5. Experimental (dots) and numerical results (line) comparison in the left, middle, and right vertical cross section of the chamber with oil for RBC for temperatures TS01 = 41.3 °C and TS16 = 30.3 °C

Conclusion

Experimental chamber has shown great flexibility. The probes are arranged so that three or four probes measure the temperature in three different vertical cross sections. This arrangement enables implementing various hydraulic fluids at different temperature regimes and switching hot and cool plate positions.

Numerical experiment was performed with the basic experimental data input. Validation is performed in the defined vertical sections, for the temperature. The values of Rayleigh number are in accordance with the velocity field obtained by the numerical experiment.

Numerically obtained values of the velocity field have shown that the vertical velocity component is in the order of magnitude of 1 cm/s in the case of the heated lower plate and 1 mm/s for the case of the heated upper plate.

For observed flow conditions, and atmospheric conditions of moderate continental climate characteristic for city of Niš (the changing temperature of the cold plate), one can conclude that the formation of characteristic connective structure takes place within the first 150 seconds.

Simulation results clearly show impact of the walls on creation of additional disturbances to the flow. In the case of the warmer upper plate stratification is expected, but due to the existence of temperature imbalances, influences of the wall roughness, tangential stresses occur which lead to the mixing of fluid layers, although the buoyancy and gravitational forces acting on the mass of the fluid are in the same direction.

Mixing occurs firstly in the corners on the side of the warmer plate, where the friction is the most influential, which is then slowly transferred to the whole fluid mass, with noticeable oscillatory repetitive structure shape in the relevant sections of the chamber.

The results obtained by the numerical simulation confirms the experimental results with the error in the range of 1-8%.

Nomenclature

a – thermal diffusivity coefficient, [m^2s^{-2}]
C – constant [–]
c_p – specific heat capacity at co. p. [$Jkg^{-1}K^{-1}$]
g – gravity acceleration, [ms^{-2}]
h – enthalpy, [Jkg^{-1}]
k – turbulent kinetic energy, [m^2s^{-2}]
L – length, [m]
p – pressure, [Pa]
P_k – turbulence production
T, t – temperature, [K, ºC]
U – main flow velocity, [ms^{-1}]
u, v, w – flow velocity, [ms^{-1}]
x, y, z – axis
$y+$ – dimensionless distance
Pr – Prandtl number
Ra – Rayleigh number

Greek symbols

α – heat transfer coefficient, [$Wm^{-2}K^{-1}$]
ε – turbulent kinetic energy dissipation, [m^2s^{-3}]
λ – thermal conductivity, [$Wm^{-1}K^{-1}$]
μ – dynamic viscosity, [Pa·s]
ν, ν_T, ν_{eff} – kinetic, turbulent, effective viscosity, [m^2s^{-1}]
Φ – general variable
Γ_Φ – diffusion term
S_Φ – source term
ρ, ρ_0 – density, initial density, [kgm^{-3}]
σ_k, σ_ε – turbulence model constants

Subscripts

i, j, k, l – co-ordinate

Acronyms

RBC – classic Rayleigh-Benard convection
RNG – renormalized group

Acknowledgment

This paper is part of the research financially supported by the Republic of Serbia Ministry of Science, Technological Development and Innovation (Contract No. 451-03-47/2023-01/ 200109).

References

[1] Rayleigh, O. M., LIX. On Convection Currents in a Horizontal Layer of Fluid, when the Higher Temperature is on the Under Side, *The London, Edinburgh, and Dublin Philosophical Magazine and Journal of Science, Sixth series*, *32* (1916), 192, pp. 529-546
[2] Block, M. J., Surface Tension as the Cause of Benard Cells and Surface Deformation Film, *Nature (London)*, *178* (1956), Sept., pp. 650-651

[3] Pearson, J. R. A., On Convection Cells Induced by Surface Tension, *Journal of Fluid Mechanics*, *4* (1958), 5, pp. 489- 500
[4] Hartmann, D. L., Tropical Convection and the Energy Balance at the Top of the Atmosphere, *Journal of Climate*, *14* (2001), 24, pp. 4495-4951
[5] Marshall, J., *et al.,* Open-Ocean Convection: Observations, Theory, and Models, *Reviews of geophysics*, *37* (1999), 1, pp. 1-64
[6] Rahmstorf, S., *Thermohaline Ocean Circulation*, Encyclopaedia of Quaternary Sciences, Edited by S. A. Elias. Elsevier, Amsterdam, The Netherland, 2006
[7] Hunt, G. R., *et al.,* The Fluid Mechanics of Natural Ventilation – Displacement Ventilation by Buoyancy-Driven Flows Assisted by Wind, *Energy and the Environment*, *34* (1999), 6, pp. 707-720
[8] Cui, H., *et al.,* Transitional Free Convection Flow and Heat Transfer within Attics in Cold Climate, *Thermal Science, 26* (2022), 6A, pp. 4699-4709
[9] Brent, A. D., *et al.,* Enthalpy Porosity Technique for Modelling Convection-Diffusion Phase Change - Application to the Melting of a Pure Metal, *Numerical Heat Transfer*, *13* (1988), 3, pp. 297-318
[10] McKenzie, D. P., *et al.,* Convection in the Earth's Mantle: Towards a Numerical Simulation, *Journal of Fluid Mechanics, 62* (1974), 3, pp. 465-538
[11] Cardin, P., *et al.,* Chaotic Thermal Convection in a Rapidly Rotating Spherical Shell: Consequences for Flow in the Outer Core, *Physics of The Earth and Planetary Interiors*, *82* (1994), 3-4, pp. 235-259
[12] Cattaneo, F., *et al.,* On the Interaction Between Convection and Magnetic Fields, *Astrophysics Journal*, *588* (2003), 2, pp. 1183-1198
[13] Glatzmaier, G. A., *et al.,* A 3-Dimensional Self-Consistent Computer Simulation of a Geomagnetic Field Reversal, *Nature*, *377* (1995), Sept., pp. 203-209
[14] Jovanović, M. M., *et al.,* Rayleigh-Benard Convection Instability in the Presence of Temperature Variation at the Lower Wall, *Thermal Science, 16* (2012), Suppl. 2, pp. S281-S294
[15] Zhou, J., Numerical Simulation of the Energy-Stable Scheme for Swift-Hohenberg Equation, *Thermal Science, 23* (2019), Suppl. 3, pp. S669-S676
[16] Jovanović, M. M., *et al.,* The Horizontal Convection of an Inclined Viscous Fluid-flow, *Innovative Mechanical Engineering,* 1 (2022), 3, pp. 49-60
[17] Chandrasekhar, S., *Hydrodynamic and Hydromagnetic Stability*, Dover, New York, USA, 1981
[18] Drazin, P., Reid, W. H., *Hydrodynamic stability*, Cambridge University Press, Cambridge, UK, 1981
[19] Bodenschatz, E., *et al.,* Recent Developments in Rayleigh-Benard Convection, *Ann. Rev. Fluid Mech.*, *32* (2000), 1, pp. 709-778
[20] Getling, A. V., *Rayleigh-Benard Convection: Structures and Dynamics*, World Scientific, Singapore, 1998
[21] Ebert, A., *et al.,* Experimental Study of Temperature Distribution and Local Heat Flux for Turbulent Rayleigh-Benard Convection of Air in a Long Rectangular Enclosure, *International Journal of Heat and Mass Transfer*, *51* (2008), 17-18, pp. 4238-4248
[22] Anderson, T. N., *et al.*, Experimental Determination of Natural Convection Heat Transfer Coefficients in an Attic Shaped Enclosure, *Int. Com. in Heat and Mass Transfer*, *37* (2010), 4, 360-363
[23] Sheel J. D., Rotating Rayleigh-Benard Convection, Ph. D. thesis, California Institute of Technology, Pasadena, Cal., USA, 2007
[24] Ayed, S., *et al.*, Experimental Study of Temperature Distribution for Turbulent Rayleigh-Benard Convection in Rectangular Tank, *Annals of Faculty Engineering Hunedoara – International Journal of Engineering*, *12* (2014), 1, pp. 117-120
[25] Bairi, A., *et al*, A Review on Natural Convection in Enclosures for Engineering Applications. The Particular Case of the Parallelogrammic Diode Cavity, *Applied Thermal Eng.*, *63* (2014), 1, pp. 304-322
[26] Pourmahmoud, N., *et al.,* Numerical Comparison of Viscosity Models on Mixed Convection in Double Lid-Driven Cavity Utilized CuO-Water Nanofluid, *Thermal Science, 20* (2016), 1, pp. 347-358
[27] El-Maghlany, W., *et al.,* Mixed Convection in an Eccentric Annulus Filled by Copper Nanofluid, *Thermal Science, 20* (2016), 5, pp. 1597-1608
[28] Astanina, M. S., *et al.,* Effect of Thermal Radiation on Natural Convection in a Square Porous Cavity Filled with a Fluid of Temperature-Dependent Viscosity, *Thermal Science, 22* (2018), 1B, pp. 391-399
[29] Laidoudi, H., *et al.,* Mixed Convection in Poiseuille Fluid from an Asymmetrically Confined Heated Circular Cylinder, *Thermal Science, 22* (2018), 2, pp. 821-834

[30] Hadjadj, S., *et al.,* Entropy Generation of Aiding Mixed Thermal Convection, Between Two Non-Parallel Vertical Plates with Uniform Temperature, *Thermal Science, 23* (2019), 2A, pp. 465-474
[31] Alkhalidi, A., *et al.,* Rarefaction and Scale Effects on Heat Transfer Characteristics for Enclosed Rectangular Cavities Heated from Below, *Thermal Science, 23* (2019), 3B, pp. 1791-1800
[32] Chen, J., *et al.,* Numerical Investigation on Saturated Boiling Flow and Heat Transfer of Mixture Refrigerant in a Vertical Rectangular Mini-Channel, *Thermal Science, 22* (2018), Suppl. 2, pp. S617-S627
[33] Wang, W., *et al.,* Analysis and Correlation of Fluid Motions in Natural Thermal Convection in a Cylindrical Vessel, *Thermal Science, 23* (2019), Suppl. 3, pp. S859-S865
[34] Laidoudi, H., Natural Convection from Four Circular Cylinders in Across Arrangement within Horizontal Annular Space, *Acta Mechanica et Automatica*, *14* (2020), 2, pp. 98-102
[35] Laidoudi, H., *et al*.: Natural-Convection of Newtonian Fluids Between Two Concentric Cylinders of a Special Cross-Sectional form, *Thermal Science, 25* (2021), 5B, pp. 3701-3714
[36] Abderrahmane, A., *et. al.*, 2D MHD Mixed Convection in A Zigzag Trapezoidal Thermal Energy Storage System Using NEPCM, *Nanomaterials, 12* (2022), 19, 3270
[37] Maneengam, A., *et. al.*, Entropy Generation in 2D Lid-Driven Porous Container with the Presence of Obstacles of Different Shapes and under the Influences of Buoyancy and Lorentz Forces, *Nanomaterials, 12* (2022), 13, 2206
[38] Asmadi, M. S., *et al.,* Nanoparticle Shape Effect on the Natural-Convection Heat Transfer of Hybrid Nanofluid Inside a U-Shaped Enclosure, *Thermal Science, 26* (2022), 1B, pp. 463-475
[39] Sharma, P. K., *et al.,* Rayleigh-Taylor Instability of Two Superposed Magnetized Viscous Fluids with Suspended Dust Particles, *Thermal Science, 14* (2010), 1, pp. 11-29
[40] Cai, W., *et al.,* Lattice Boltzmann Simulation of Rayleigh-Benard Convection in Enclosures Filled with Al_2O_3-Water Nanofluid, *Thermal Science, 22* (2018), Suppl. 2, pp. S535-S545
[41] Aliouane, I., *et. al.*, Investigation of the Flow and Thermal Fields in Square Enclosures: Rayleigh-Benard's Instabilities of Nanofluids, *Ther. Sci. and Eng. Progress*, *25* (2021), 100959
[42] Bairi, A., *et al*, Numerical and Experimental Study of Natural Convection in Tilted Parallelepipedic Cavities for Large Rayleigh Numbers, *Experimental Thermal and Fluid Science*, *31* (2007), 4, pp. 309-324
[43] Ayed, S., *et al*., Instability of Rayleigh-Benard Convection Affected by Inclined Temperature Variation, *Proceedings*, 12th International Conference DEMIC 2015, Chapel Hill, N. C. USA, pp. 373-378
[44] Kenjeres, S., Hanjalic, K., Transient Analysis of Rayleigh-Benard Convection with a RANS Model, *International Journal of Heat and Fluid-flow*, *20* (1999), 3, pp. 329-340
[45] Kenjeres, S., *et al.,* Reorganization of Turbulence Structure in Magnetic Rayleigh-Benard Convection: A T-RANS Study, *Journal of Turbulence*, *1* (2000), 8, pp. 1-22
[46] Sun, C., *et al.,* Experimental Studies of the Viscous Boundary Layer Properties in Turbulent Rayleigh-Benard Convection, *Journal of Fluid Mechanics, 605* (2008), May, pp. 79-113
[47] Shishkina, O., *et al.,* Thermal Boundary Layer Equation for Turbulent Rayleigh-Benard Convection, *Physical Review Letters, 104* (2008), 036311, pp. 1-5
[48] Reeuwijk, M. van, *et al.,* Wind and Boundary Layers in Rayleigh-Benard Convection, I. Analysis and Modeling, *Physical Review, E 77* (2010), 036311, pp. 1-15
[49] Reeuwijk, M. van, *et al.,* Wind and boundary layers in Rayleigh-Benard Convection. II. Boundary Layer Character and Scaling, *Physical Review, E 77* (2010), 036311, pp. 1-10
[50] Shi, N., *et al.,* Boundary Layer Structure in Turbulent Rayleigh-Benard Convection, *Journal of Fluid Mechanics, 706* (2012), June, pp. 5-33
[51] Zhou, Q., *et al.,* Measured Instantaneous Viscous Boundary Layer in Turbulent Rayleigh-Benard Convection, *Physical Review Letters, 114* (2015), 114302, pp. 1-4
[52] Wang, Y., *et al.,* Boundary layer fluctuations in turbulent Rayleigh–Benard convection, *Journal of Fluid Mechanics*, 840 (2018), 3, pp. 408-431
[53] Ching, E. S. C., *et al*., Velocity and Thermal Boundary Layer Equations for Turbulent Rayleigh-Benard Convection, *Physical Review Research*, *3* (2019), 033037-1, pp. 1-7
[54] Huang, M., *et al.,* Heat Transport and Temperature Boundary-Layer Profiles in Closed Turbulent Rayleigh-Benard Convection with Slippery Conducting Surfaces, *Journal of Fluid Mechanics, 943* (2022), A2, pp. 1-21

[55] Nourollahi, M., *et al.,* Numerical Study of Mixed Convection and Entropy Generation in the Poiseulle-Benard Channel in Different Angles, *Thermal Science, 14* (2010), 2, pp. 329-340
[56] Akrour, D., *et al.,* A Theoretical and Numerical Study of Thermosolutal Convection: Stability of a Salinity Gradient Solar Pond, *Thermal Science, 15* (2011), 1, pp. 67-80
[57] Newell, A. C., *et al*., Order Parameter Equations for Patterns, *Annual Review of Fluid Mechanics*, *25* (1993), 1, pp. 399-453
[58] Ayed, S., *et al*., Experimental and Analytical Solution for Rayleigh-Benard Convection, *International Journal of Computation and Applied Sciences IJOCAAS*, *3* (2017), 2, pp. 224-232

Paper submitted: June 7, 2023
Paper revised: July 17, 2023
Paper accepted: July 30, 2023